Hindawi
Shock and Vibration
Volume 2018, Article ID 2059784, 12 pages
https://doi.org/10.1155/2018/2059784

Research Article

Vibration of Shaft System in the Mixed-Flow Pump Induced by the Rotor-Stator Interaction under Partial Load Conditions

Wei Li,[1] **Leilei Ji**,[1] **Weidong Shi**,[1,2] **Yulu Wang**,[1] **Ling Zhou**,[1] **and Xiaoping Jiang**[1]

[1]*Research Center of Fluid Machinery Engineering and Technology, Jiangsu University, Zhenjiang 212013, China*
[2]*College of Mechanical Engineering, Nantong University, Nantong 226019, China*

Correspondence should be addressed to Wei Li; lwjiangda@ujs.edu.cn, Leilei Ji; jileileidemail@163.com, and Weidong Shi; wdshi@ujs.edu.cn

Received 10 May 2018; Accepted 13 July 2018; Published 26 August 2018

Academic Editor: Marc Thomas

In order to reveal the relationship between rotor-stator interaction-induced unsteady flow and the shaft vibration of the mixed-flow pump, PIV (particle image velocimetry) and axis orbit experiments were carried out synchronously in a mixed-flow pump under designed flow rate ($1.0Q_{des}$) and the partial load conditions ($0.4Q_{des}$ and $0.2Q_{des}$). The distribution of the relative velocity and the vorticity in the rotor-stator interaction region at a certain position of the mixed-flow pump impeller was captured; the axis orbit diagram and the time-domain diagram of shaft system were acquired as well. Besides, the waterfall diagrams of the frequency spectrum under different flow rate conditions were compared. The results show that the backflow and the flow separation phenomenon appear in the rotor-stator interaction flow field under the partial load condition, indicating the flow instability. The medium-frequency exciting force and high-frequency exciting force induced by these unstable flows resulting from the rotor-stator interaction are the main factors to intensify the shaft vibration at the power frequency. The rotor-stator interaction under partial load condition is the main reason for the deterioration of shaft system vibration. The 2X frequency also affects the axis orbit in a low level, while other frequencies have less influence on the shaft vibration. The research results can provide the reference and theory instruction for revealing the operating characteristic of mixed-flow pump when it operates under partial load conditions and to reduce or to prevent the deterioration of vibration of shaft system.

1. Introduction

The mixed-flow pump is widely used in fields such as agricultural irrigation, urban water supply, thermal and nuclear power plants, and so on. Due to the diversity of operating conditions and the change of the system load, the mixed-flow pump often operates at off-design conditions. Working at off-design conditions especially at small flow discharges, the internal flow of the mixed-flow pump becomes more complicated, with the appearance of the backflow and flow separations [1–3]. These unsteady flows bring negative effect to the operating pump, and the most obvious impact is the increase on the shaft system vibration and the periodical radical and axial forces [4–7]. At some extreme situations, the entire pump unit would break down as a result of the resonance [8–10]. So, lots of the literatures about the vibration of the pump operating at various flow rate conditions are reported in order to enhance the operational stability or reduce the vibration of the mixed-flow pump shaft system. Wang et al. [11] studied the pressure fluctuation and vibration in mixed-flow pumps, and the results show that the peak value of pressure fluctuation decreased gradually with the increase of flow rate and the vibration frequency occurred at shaft frequency and its multiple shaft frequency. van Esch et al. [12–14] researched the relation between the instability and the unsteady hydraulic forces in order to attenuate the vibration resulting from the rotating stall and unstable operation. Gros et al. [15, 16] conducted researches on the hydrodynamic instabilities of a centrifugal pump concerning part-load operating points. An unstable characteristic appeared at part load, and also the consequence is an unstable local head drop

of the performance curve and the singularity exhibits a positive slope in the decreasing performance curve. Ding et al. [17] found the recirculation generated in the suction pipe and the reverse flow occurred in the impeller passages when the pump runs at low flow rates, making the total efficiency deviating from the design condition. Zhou et al. [18] captured vertical flow and recirculation flow patterns in a compact return diffuser under strong part-load conditions, and at the same time, large flow separation and backflow were found numerically and experimentally under the part-load flow conditions. Tan et al. [19] investigated the unsteady flows in a centrifugal pump volute at noncavitation and cavitation under part-load condition. It showed that, under cavitation conditions, the flow field in pump volute was with large pressure gradient and intensive vortex movement. Pedersen et al. [20, 21] detected the large recirculation cell blocking the inlet to the stalled passage, while the strong relative eddy dominated the remaining parts of the passage by means of particle image velocimetry (PIV) and laser Doppler velocimetry (LDV) measurements in a six-bladed shrouded centrifugal pump impeller at design and off-design conditions. In the previous published papers [22], based on the numerical calculation and experiment, the vibration characteristics of the impeller at multiconditions in mixed-flow pump under the action of fluid-structure interaction were investigated in depth. However, the generation of the unsteady flow is more under the part-load condition, and other factors also take great impacts.

It is well known that, due to the special structure of the mixed-flow pump, there is a gap between the impeller and guide vane blade. The flow in the gap region shows severely unsteady feature as the result that the impeller is rotating while the guide vane is stationary when the pump is operating. In addition, the unsteady flow characteristic would cause strong pulsating force of significant size on both the impeller and guide vanes. And this phenomenon is called the rotor-stator interaction of flow in the mixed-flow pump. Thus, except for the unsteady flow of the pump when pump operates at partial load condition, the periodic instability caused by the internal rotor-stator interaction further deteriorates the flow field and operation condition. Even though the unsteady flow feature that results from partial load condition has been investigated deeply in the turbomachinery, compressor, and fan [23–25], there are few reports about the rotor-stator interaction or the shaft system vibration caused by the rotor-stator interaction of the mixed-flow pump under the circumstance of partial load condition, and the relationship between the shaft vibration and rotor-stator interaction flow is also not revealed. Many scholars just focus on the hydrodynamic instabilities caused by unsteady characteristic of rotor-stator interaction flow or the energy loss of the pump running at partial load condition. For instance, Rodriquez et al. [26] theoretically studied the onset of vibrations by rotor-stator interaction based on a blade encounter model, and the frequency of vibration and the whirl direction of the force on the impeller were assessed for different combinations of rotor and stator blades. Dring et al. [27] divided the rotor-stator interaction into two mechanisms: potential flow interaction and wake interaction, and both of the interactions will occur and influence each other if the gap between the impeller blades and guide vanes is in a certain scale. Tsukamoto et al. [28–30] researched the rotor-stator interaction in a diffuser pump with the vortex method and pressure fluctuation measurement, and unsteady hydrodynamic forces excited by the interaction between the impeller and the vaned diffuser with the same number of vanes as impeller were studied as well. Zhang et al. [31] used CFD method to study pressure pulsation induced by rotor-stator interaction of a general mixed-flow pump. They found the vortex shedding or backflow from the impeller blade exit has the same frequency as pressure pulsation, but there are phase differences.

Nevertheless, the above research work did not associate the rotor-stator interaction between the impeller and diffuser with the operating condition of a pump, especially of a mixed-flow pump. Therefore, in order to get some knowledge of the relationship between the shaft vibration and internal unsteady flow coming from the influence of rotor-stator interaction and change of flow rate conditions, the axis orbit and particle image velocimetry (PIV) measurements of a mixed-flow pump were conducted under partial flow rate condition in this paper. Not only the vibration of shaft system could be got hold of accurately but also the vibration deterioration induced by the hydraulic force under partial flow rate condition could be prevented. Thus, based on the PIV technology, the rotor-stator interaction flow fields of mixed-flow pump are measured under the design flow rate condition and the two low flow rate conditions. At the same time, based on the Bentley 408 data acquisition system, the axis orbit of mixed-flow pump is synchronously acquired. By analyzing the internal flow characteristics of the mixed-flow pump and the time-domain diagram and frequency spectrum of axis orbit under the partial flow rate condition, the mechanism of the shaft vibration induced by the rotor-stator interaction under partial flow rate condition is revealed. Also, the changing law of the axis orbit under the partial flow rate condition is discussed which would provide the theoretical foundation for reducing or preventing the deterioration of vibration of mixed-flow pump.

2. Research Object

2.1. Experimental Model. The model of the mixed-flow pump in this study is shown in Figure 1. Figure 1(a) shows the impeller of the mixed-flow pump and the hub and blades are painted with black pigment. Figure 1(b) shows the impeller chamber wrapping the impeller and guide vane, which was made of transparency poly methyl methacrylate and its refractive index is close to the water in order to observe clearly. The parameters of the mixed-flow pump model are illustrated in Table 1. The design flow rate $Q_{des} = 380\ m^3/h$, head $H_{des} = 6\ m$, rotating speed $n_{des} = 1450\ r/min$, specific speed $n_s = 480$, the number of impeller blades $Z = 4$, the tip clearance $t = 0.5\ mm$, and the number of guide vane blades $Z_g = 7$.

3. Experiments

3.1. General Energy Performance Measurement. The experimental measurements were conducted on a 250-caliber

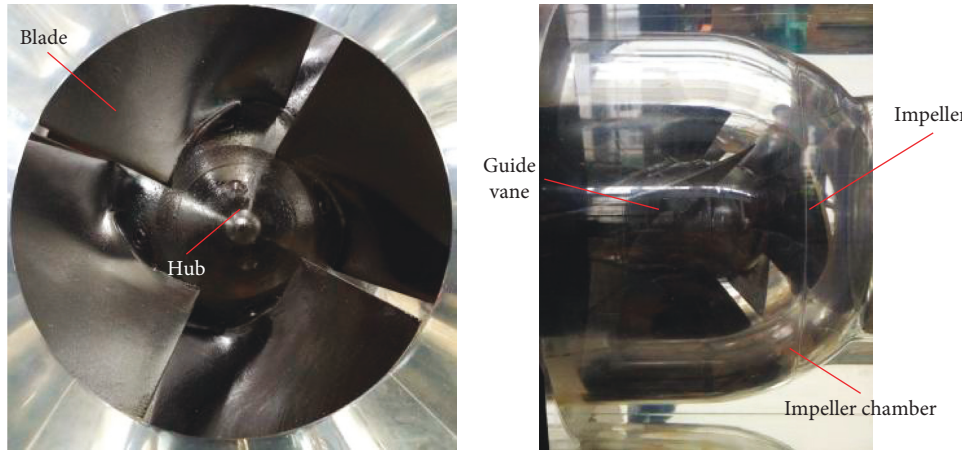

Figure 1: Mixed-flow pump model. (a) Impeller of mixed-flow pump. (b) Transparent chamber of mixed-flow pump.

Table 1: Specifications of the investigated pump.

	Variable name	Value
Impeller		
Number of blades	Z_i	4
Inlet radius	R_1	92.6 mm
Outlet radius	R_2	121.6 mm
Inlet blade angle	β_1	53.5°
Outlet blade angle	β_2	58.4°
Diffuser		
Number of blades	Z_d	7
Inlet radius	R_3	133.3 mm
Outlet radius	R_4	140.9 mm
Inlet blade angle	α_3	24.0°
Outlet blade angle	α_4	26.0°
Design operating point		
Volume flow rate	Q_{des}	380 m^3/h
Rotating speed	n_{des}	1450 r/min
Delivery head	H_{des}	6 m
Specific speed	n_s	480

closed mixed-flow pump test bench in Research Center of Fluid Machinery Engineering and Technology, Jiangsu University. The test bench meets the accuracy requirement of first class, and the experiment equipment is shown in Figure 2. The energy performance parameters of the model pumps are measured by different devices. The ZJ-type instrument produced by Shanghai-standard Intelligent Terminal Co. Ltd., with precision 0.2, was used for the torque and the tachometric measurement. The LWGY-type turbine flowmeter produced by Shanghai ZiYiJiu Automatic Instrumentation Co. Ltd., with precision 0.5, was set in the system to measure the flow rate. Besides, the MPM-type pressure sensor produced by Mike Co. Ltd., with 0.5% FS precision, was equipped at the inlet and outlet of the mixed pump to measure the flow rate. Finally, the HSJ-2010 hydraulic Machinery tester was used to acquire experimental data from the abovementioned sensors, and all the signals were then transported from HSJ-2010 hydraulic Machinery to the computer.

In the beginning of the experiment, the opening degree of inlet and outlet valves in test pipe was adjusted to the maximum and then turned on the HSJ-2010 hydraulic machinery tester and adjusted the software to record data. After that, the motor is turned on and the outlet valve opening degree was gradually reduced to make sure that the reading of flowmeter is stable at $1.0Q_{des}$ (380 m^3/h) and the rotating speed of mixed-flow pump can stabilize at 1450 r/min. The energy performance parameters are recorded, respectively. After collecting enough data, the power and the units are shut off. The next experiment is conducted after the fluid in the pipeline becomes steady again. In order to get the data in the experiment of partial flow rate condition, the experimental data at $0.4Q_{des}$ ($Q = 152$ m^3/h) and $0.2Q_{des}$ ($Q = 76$ m^3/h) are measured, respectively, and the experimental stages are the same as abovementioned.

3.2. PIV Measurement of Rotor-Stator Interaction Flow Field. The PIV measurement in rotor-stator interaction flow field of mixed-flow pump is conducted in the process of energy performance test. As the testing results are primarily influenced by the calibration accuracy in PIV test, in order to improve the test accuracy and to avoid troubles in disassembly of the pump, a calibration tank was used for calibrations of the PIV tests. As shown in Figure 3, a tank with the same shape and size is made for calibration. The tank was open on the top for the purpose of filling water and placing the ruler. Before the test, the following procedures were operated. As shown in Figure 3(a), the calibration tank was adjusted horizontally after it had been placed on a fixed bracket at the beginning. The leveling instrument makes sure the inlet and outlet of the calibration tank vertical to the ground. The external side of the camera for the tank was thereafter adjusted to the vertical plane of the surface of the impeller chamber located on the same side. In the following, as shown in Figure 3(b), the leveling instrument was placed on the top surface of a base with the same curvature as the calibration tank. The end surface of the leveling instrument

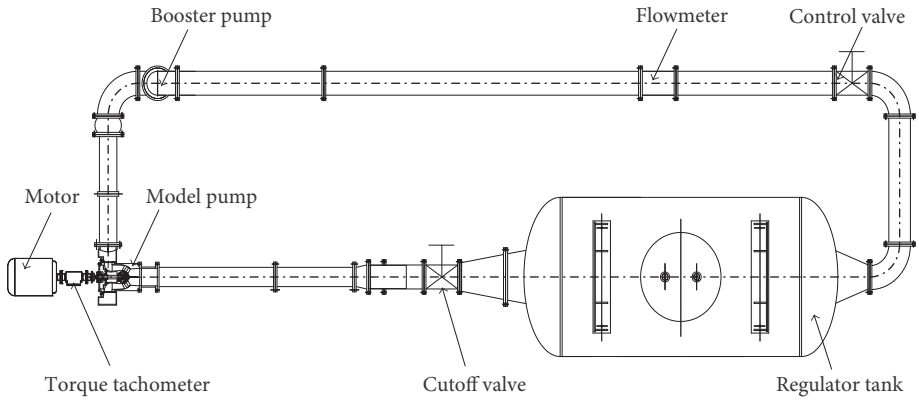

Figure 2: Experimental setup.

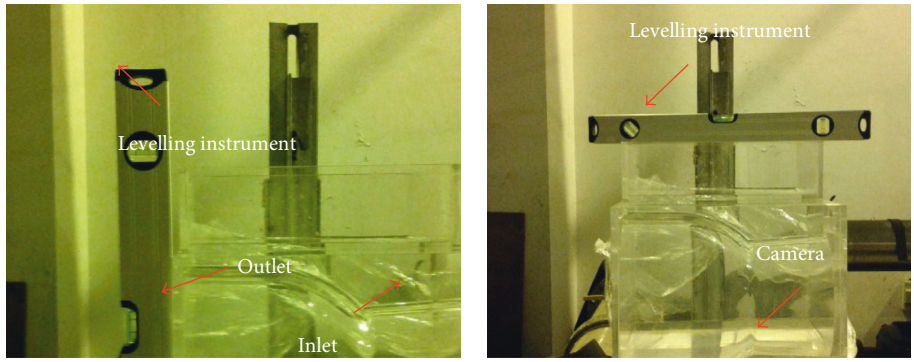

(a) (b)

Figure 3: Calibration tank and calibration process. (a) To adjust the side surfaces in the same vertical plane. (b) To adjust the end surface in the horizontal plane.

containing scales was then adjusted in accordance with the shooting plane. The camera was finally moved in the same horizontal plane as the leveling instrument.

During the PIV measurement, the experimental apparatus was mainly composed of TSI's US commercial PIV system. The major apparatus and system include YAG200-NML-type pulse laser, PIV specialized 630059POWERVIEW 4MP-type cross-frame CCD camera, 610035-type synchronous control system, 610015-SOL optical arm and light sheet system, image acquisition and analysis software Insight 3G, and so on. The high-quality solid aluminum oxide was selected as tracer particles for its relatively better fluid following quality, a particle with 20 μm–60 μm diameter and a density of 1050 kg/m^3.

The concentration and distribution of the tracer particles in the fluid are good enough to meet the requirements to obtain the image information of flow field, as shown in Figure 4. The zone marked with yellow line is the rotor-stator shooting section, and the impeller blade and guide vane are also shown in Figure 4. To make the shooting section of the flow field area big enough, the largest rotor-stator shooting section is chosen as the shooting plane when the impeller rotates at a certain phase angle. The sketch map of the shooting section is shown in Figure 5, and the layout of the PIV experimental test is also shown in Figure 5.

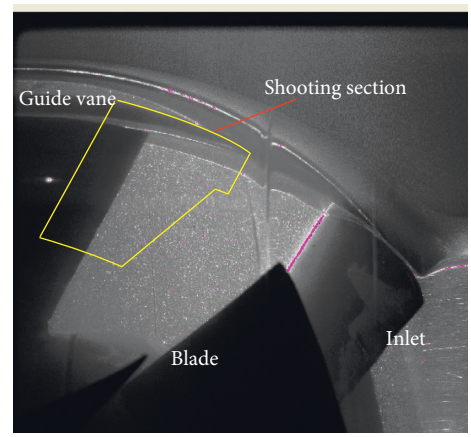

Figure 4: Tracer particle distribution in the shooting section.

In the shooting process, the frame number of the images is set as 500. After shooting was completed, self-correlation processing is conducted on the 500 frame images of tracer particles absolute velocity field by the Insight 3G software. The instantaneous relative velocity vector of each image is obtained and then imported into TECPLOT software to conduct the calculation processing for the relative velocity field and other fields in each instantaneous flow. The

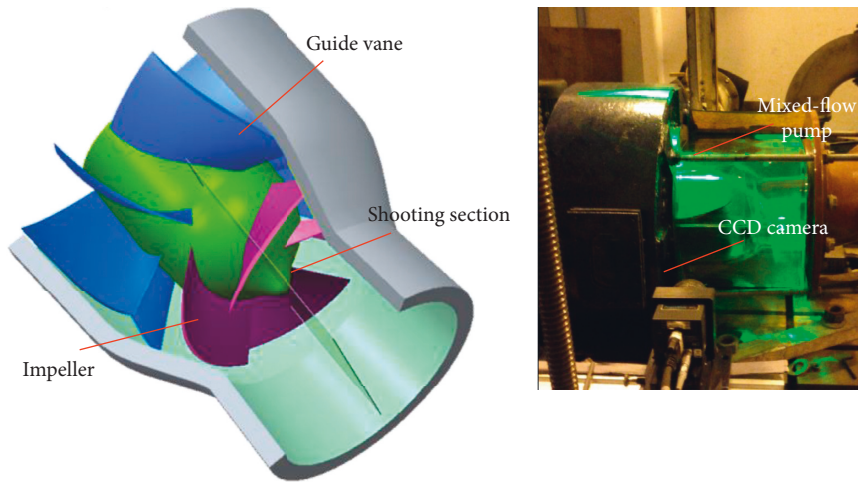

Figure 5: Sketch map of shooting section (a) and the layout of PIV experimental test (b).

requirements and experimental procedures of the PIV experiment are shown in [32].

3.3. Vibration Measurement of Shaft System of Mixed-Flow Pump. Similarly, the shaft vibration measurement of mixed-flow pump is also conducted synchronously with the energy performance test. The shaft vibration signal of mixed-flow pump under the partial flow rate condition is collected by the Bentley 408 data acquisition system which is composed of the 408 dynamic signal processing equipment and the ADRE Sxp software. The 3300 XL 8 mm eddy current displacement sensor used in this experiment consists of eddy current probe, preamplifier, and extension cord. The diameter of the eddy current probe is 8 mm and its type is 330130-040. The type of the preamplifier is 330180-50 and the length of extension cable is 4 m. The 45# steel was used as the calibration object. The sensor gap voltage is −10 V, the sensitivity of the 45# steel is 7.87 V/mm, and the measurement range is from −2 mm to +2 mm. The sensor should be installed in linear midpoint to make sure that the absolute value of the extreme measurement value to be the same.

During the measurement process, as the rotation error of mixed-flow pump rotor is larger than the roundness error, the shape error of the rotor shaft can be ignored. The method used in this experiment to monitor the vibration situation of rotor is a two-way dynamic measurement method, which is mentioned in [33]. The data collection and detection system were connected according to the requirement of the experiment, and the monitor points are set near the side where the coupling and motor are connected. The eddy current displacement sensor and keyphasor transducer are also installed correctly according to the requirement. Then, all the facilities are connected to the 408 dynamic signal processing equipment. The two eddy current displacement sensors are installed vertical to each other, and the distance between the probe and rotor shaft in eddy current displacement sensor is 1 mm. The keyphasor is installed 5 mm away from the reflective sheeting attached in the rotor shaft and kept vertical to the shaft. The axis orbit measurement and test arrangement are shown in Figure 6.

4. Results and Analysis

4.1. Results of Energy Performance Test. Three trials of energy performance test of mixed-flow pump model were preceded, and the mean external characteristic parameters of mixed-flow pump acquired in the experiment are shown in Table 2. It can be seen that the inlet pressure and outlet pressure increase with the decrease of the flow rate. Also, the absolute value of pressure difference between the inlet and outlet increases, namely, the pump head increases when the flow rate decreases. Meanwhile, some small extent of increase of the torque and shaft power also emerges with the decrease of the flow rate, which indicates that the hydraulic load increases with the decrease of the flow rate.

4.2. Analysis of PIV Experiment Results. Within this section, the comparative analysis of the distribution of the relative velocity and the vorticity was conducted at the outlet zone of the impeller when the flow rate condition is $1.0Q_{des}$ or at the small flow rate condition of $0.4Q_{des}$, $0.2Q_{des}$.

It can be seen from Figures 7 and 8, when the mixed-flow pump operates at the designed condition, the flow loss in the mixed-flow pump is at a low level and the streamlines in the shooting section appeared oblique outflow trend. However, due to the influence of the leakage flow on the front blade rim and the flow separation on the blade surface, some vortex structures exist within a small zone near the end wall of the impeller outlet and the hub surface. Meanwhile, as shown in the vorticity field (Figure 8), the strength of vortex core is not very high at the design flow rate condition, which indicates that the limited impact on the flow field and the influence of the vortex structure are not intensive. Thus, from the streamlines trend and the vortex region, it can be known that the rotor-stator interaction between the impeller and guide vane did not affect the flow field as much as the

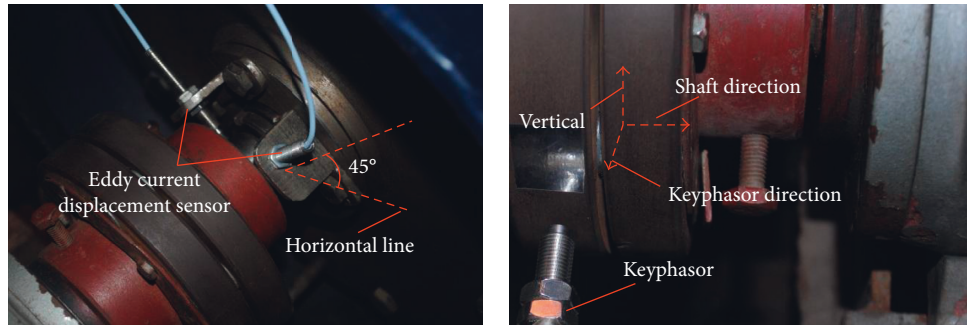

(a) (b)

Figure 6: Measurement of axis orbit. (a) Position of eddy current displacement sensor. (b) Position of keyphasor.

Table 2: Results of energy performance.

Parameters	$1.0Q_{des}$	$0.4Q_{des}$	$0.2Q_{des}$
Inlet pressure(kPa)	17.99	23.72	30.44
Outlet pressure (kPa)	71.96	104.27	123.32
Rotating speed(r/min)	1450.88	1447.7	1448
Torque (N·m)	58.78	60.39	70.25
Shaft power (kW)	8.93	9.15	10.65

leakage flow or the geometry of the impeller and guide vane blade. When the mixed-flow pump operates at the partial flow rate condition, the flow loss increases obviously in the mixed-flow pump and the flow instability also increases significantly. Compared with the design flow rate condition, the fluid velocity increases near the end wall area and the streamlines are in a mass within the interference zone between the impeller outlet and the guide vane inlet at $0.4Q_{des}$. The backflow phenomenon happens obviously at the position of guide vane inlet. From the vorticity field, the vortex intensity is relatively high, while the swirling direction is adverse near the end wall of guide vane inlet and the hub surface. At $0.2Q_{des}$, the flow instability further increases, the backflow at the position of guide vane inlet becomes more obvious, and the impact area enlarges evidently. At the same time, the vorticity value rises near the end wall and the hub surface of the impeller outlet. Comparing the three load conditions, it can be found that the negative vorticity center near the hub moves away from the hub surface and is much closer to the impeller outlet. Oppositely, the positive vorticity center moves from the impeller outlet to the guide vane inlet. Those flow characteristics represent the instability in the rotor-stator interaction zones, while the secondary flow and backflow are further intensified with the drop of the flow rate. Overall, differing from the design flow rate condition, at the partial flow rate condition, the flow instability increases and the backflow phenomenon happens obviously at the position of guide vane inlet. Meanwhile, negative vorticity with high value appears near the position of hub surface. Consequently, the rotor-stator interaction between the impeller and guide vane under the partial flow rate conditions is obvious. In addition, with the reduction of the flow rate, the strength of the rotor-stator interaction increases which is implied by the interaction flow field. It is also well known that the flow instability often happens in accompany with the vibration and noise. The generated fluid excited vibration would have a harmful impact on the stable operation of the shaft system. Therefore, it is meaningful and necessary to do some research to link the shaft vibration to the rotor-stator interaction at the partial flow rate condition.

4.3. Analysis of Axis Orbit Experiment Results

4.3.1. Time Domain of Original Rotor Axis Orbit. The shaft vibration of the mixed-flow pump could be reflected by the axis orbit diagram combined by the two direction signals that are mutually perpendicular. The faults of the mixed-flow pump can be detected by analyzing the data that is processed from the original axis orbit signals using special method. In this paper, in the process for filtering and purifying the original axis orbit waveform, the Butterworth band-pass filter, integrated in the ADRE Sxp software, is chosen to purify the original axis orbit signal. The characteristics of the Butterworth filter are that the frequency response in the pass band is uttermost flat and has no ups and downs, which gradually decreases to zero in the suppressed frequency band. The original axis orbit diagram of the mixed-flow pump rotor and its time-domain diagram acquired within 0.15 s at $1.0Q_{des}$, $0.4Q_{des}$, and $0.2Q_{des}$ are demonstrated in Figure 9.

It can be found that the original axis orbits at different flow rate conditions are not smooth and integral circles but in the shape like number "8" with zigzagged sharp corners. According to fault diagnosis literatures of rotating machinery [34–38], this characteristic indicates that the typical misalignment fault exists in the rotor shaft of the mixed-flow pump during the operation. As the monitor position is closed to the bearing, the most possible reason can be that the rotor and the bearing are out of tolerance during centering. The original axis orbit always accompanies with the constantly changing zigzagged sharp corners, namely, the "burrs" are quite more, which reflects that friction inevitably exists between the rotor and the shaft-bearing pair or some other high-order harmonics components such as the hydraulic vibration and noise in the pump have a great influence on the axis orbit. As the flow rate decreases, the zigzagged sharp corners become bigger resulting from the

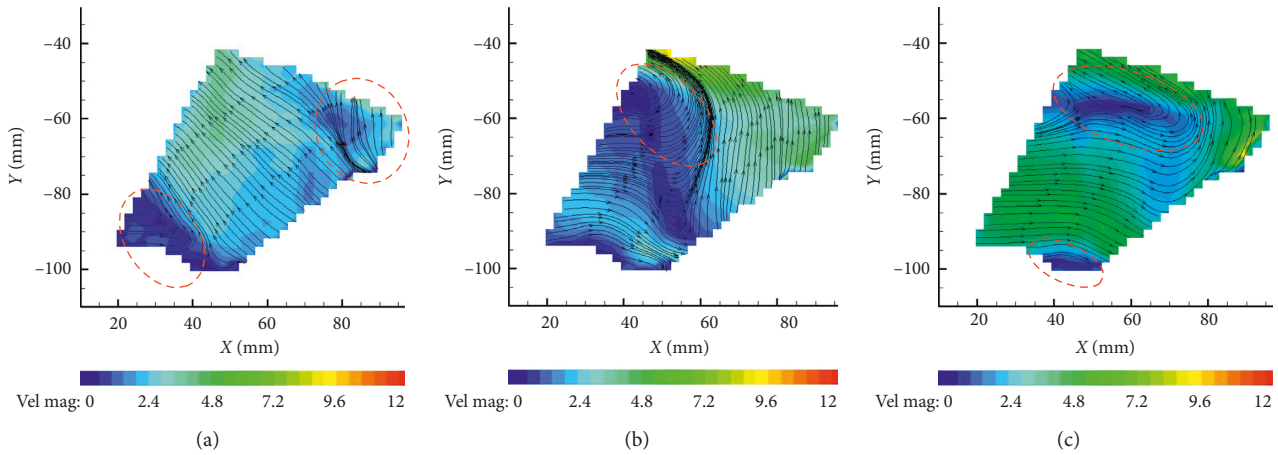

Figure 7: Streamline distribution of shooting section under different flow rate conditions. (a) $1.0Q_{des}$, (b) $0.4Q_{des}$, and (c) $0.2Q_{des}$.

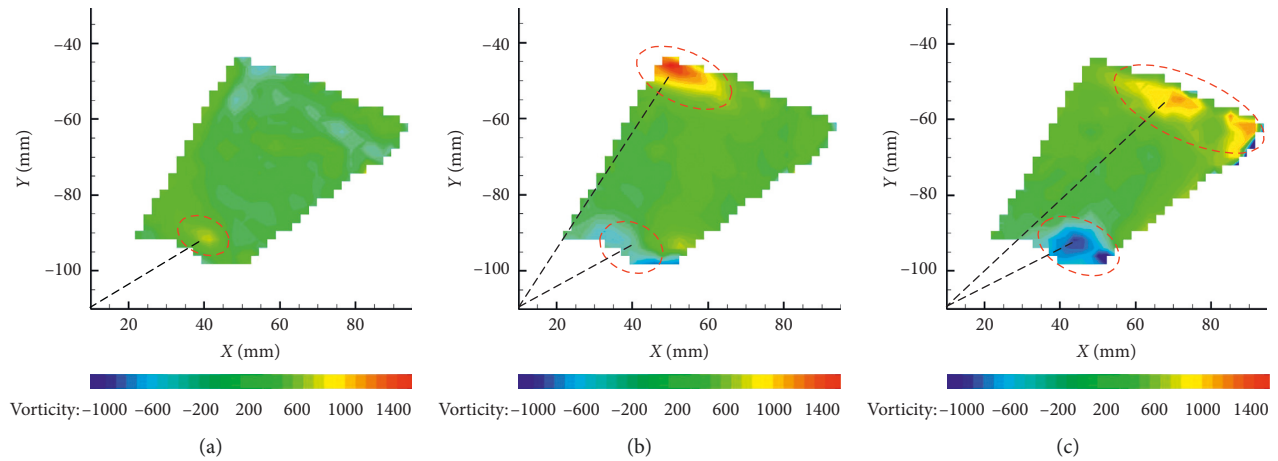

Figure 8: Vorticity distribution of shooting section under different flow rate conditions. (a) $1.0Q_{des}$, (b) $0.4Q_{des}$, and (c) $0.2Q_{des}$.

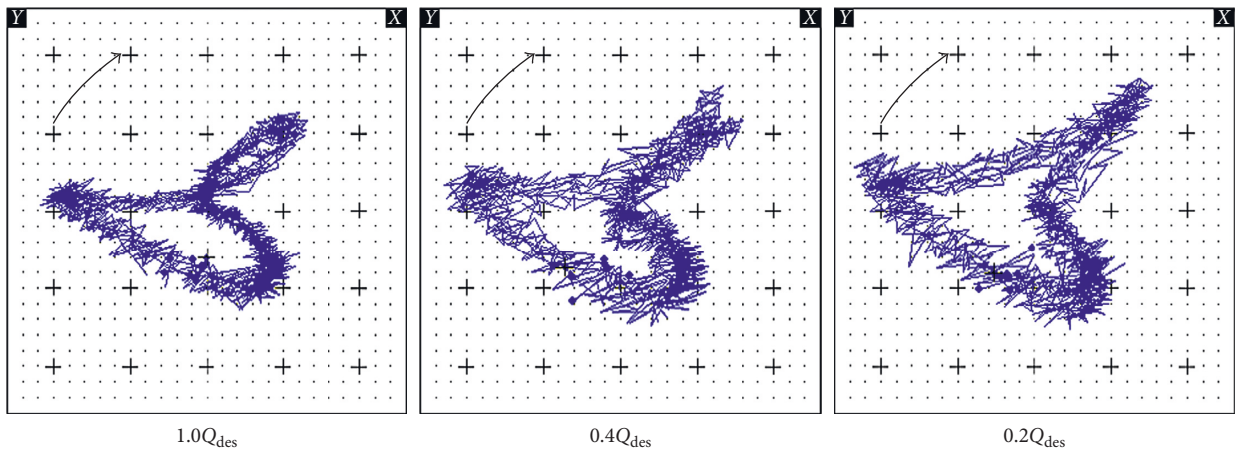

(a)

Figure 9: Continued.

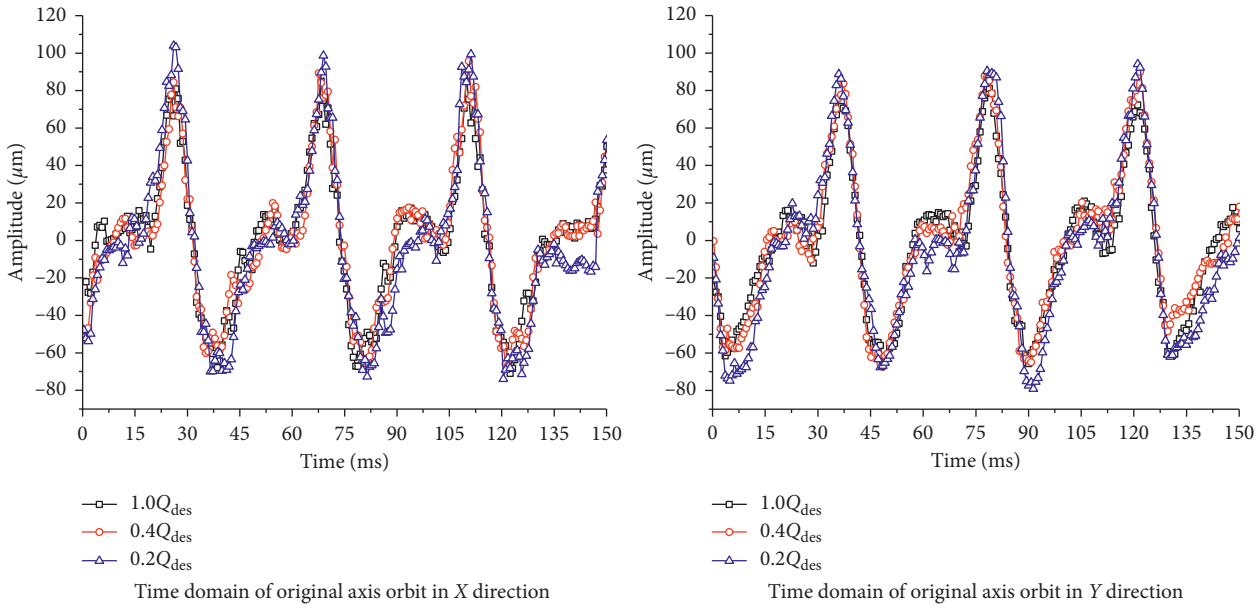

(b)

Figure 9: Axis orbit and time-domain diagram of the original. (a) Original axis orbit diagram. (b) Time-domain diagram of axis orbit.

severe rotor-stator interaction under partial flow rate conditions, which leads to more adverse effects. Moreover, from time-domain diagram of the original axis orbit in X direction and Y direction, it can be found that the time-domain diagram of the axis orbit in X direction is aberrant sinusoidal wave, on which the secondary peaks present at the mains frequency, while the time-domain diagram of the axis orbit in Y direction is aberrant cosine wave and the phase difference between the X direction and Y direction of the axis orbit time-domain diagram is exactly 1/4 cycle. Comparing the time-domain diagram at three flow rate conditions, it could be found that the rotor-stator interaction under the partial flow rate condition is the most important influencing factor of the chaotic axis orbit and the high fluctuation amplitude, but that is relatively low under the design flow rate condition. In the changing process from the design flow rate condition to $0.2Q_{des}$, the peak value of the time-domain diagram in X direction and Y direction keeps increasing with the decrease of the flow rate. Accordingly, the amplitude value of the compounded axis orbit is always increasing which indicates that the vibration of the shaft system deteriorates when the operating point of mixed-flow pump moves to the partial load condition. It is corresponded to the experience-based judgment that the rotor system would lose stability easily when the pump operates under the partial load condition.

4.3.2. 1X Frequency Axis Orbit and Its Time-Domain Diagram. After the decomposition and purification, the 1X frequency of the axis orbit and its time-domain diagram were obtained. As shown in Figure 10, the interference from the ultrahigh harmonic signal such as the noise and electromagnetic are ruled out in the original signal of the axis orbit. It can be found from the 1X frequency axis orbit after purification that the shape of the 1X frequency the axis orbit under three flow rate conditions is approximate to a circle and the circle is drawn in a counterclockwise direction, which is on the contrary of the rotor rotation direction. According to previous studies [39–42], it can be judged that the difference of the bearing stiffness in different directions is very small, and the influence of the bearing factor on a frequency doubling can be neglected. Meanwhile, it can be judged that the mixed-flow pump has the counterclockwise arc-shaped rotary motion in the operating process, namely, the rotor exists the power frequency vibration caused by the unbalance of the rotor. As the flow rate decreases, the profile of the axis orbit varies from small to large and the peak value of the 1X frequency waveform in the X direction and Y direction gradually increases. All indicate that the power frequency vibration caused by rotor unbalance increases with the decrease of the flow rate condition, and the peak value of shaft system vibration of the power frequency occurs at $0.2Q_{des}$. In the X direction, the amplitude of the fluctuation at $0.2Q_{des}$ increases by 25.4% compared to that at design flow rate point. In the Y direction, the amplitude of the fluctuation at $0.2Q_{des}$ increases by 21.3% compared to that at the design flow rate point. The amplitude of fluctuations at $0.2Q_{des}$ increase almost 0.2 times compared to that at the design flow rate point. Thus, when the flow rate condition drops down to a partial flow rate condition, the abovementioned recirculation, secondary flow, and other different scale vortex will appear inside the rotor-stator interaction field of the mixed-flow pump, the medium-frequency and high-frequency exciting force induced by these unstable flow may be main reasons for the deterioration of shaft system vibration at the power frequency. Therefore, in order to improve the reliability of the shaft system and the

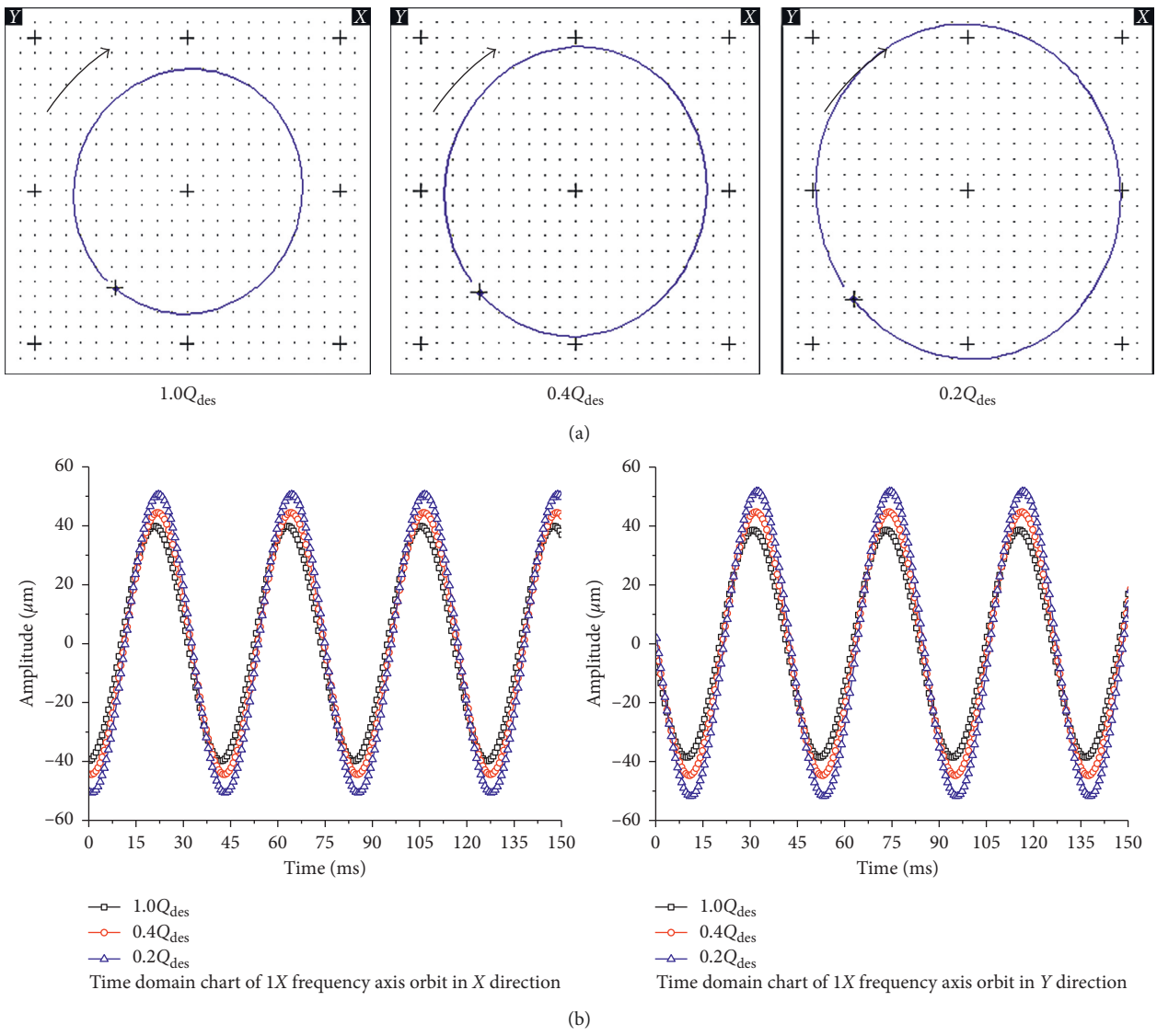

FIGURE 10: Axis orbit and time-domain diagram of 1X frequency axis orbit. (a) Axis orbit diagram of 1X frequency. (b) Time-domain diagram of 1X frequency axis orbit.

pump life span, the mixed-flow pump should avoid running in small flow rate conditions.

4.3.3. Analysis of Axis Orbit Frequency Spectrum. The frequency spectrum of the axis orbit in the X direction and Y direction at 1.0Q_{des}, 0.4Q_{des}, and 0.2Q_{des} is plotted, which is shown in Figure 11. The rated speed n_{des} of the mixed-flow pump is 1450 r/min, so its rotating frequency f is 24.17 Hz. It can be seen from Figure 11 that the energy concentration in the frequency spectrum indicates the 1X frequency and the 2X frequency of the axis orbit occupying the main vibration energy while the triple and quadruple frequency share little. Comparing the frequency spectrum distribution at different flow rate conditions, the amplitudes of 1X frequency show more differences, while the amplitudes of 2X frequency are slightly different, and the amplitudes of other frequencies have little difference. Under the three operating conditions, the amplitude of the 1X frequency and the 2X frequency is the smallest at 1.0Q_{des}, but the amplitude of the 1X frequency and the 2X frequency is increasing constantly with the decrease of the flow rate. At 0.2Q_{des}, the amplitude of the 1X frequency and the 2X frequency is largest. The 1X frequency characterizes the dynamic unbalance of the shaft system, while the 2X frequency represents the misalignment of the rotor. It could be known that, with the decrease of the flow rate, the unbalance of the shaft system of the mixed-flow pump increases, which leads to the increase of the vibration amplitude of the shaft system, especially the vibration of the shaft system influenced obviously by the rotor-stator interaction under the partial load conditions. At the same time, the degree of misalignment of the shaft system also increases with the decrease of the flow rate conditions. The results show that the growth of the flow rate makes the radial offset and misalignment of the shaft system increase, and also the vibration increases. The rotor-stator interaction under

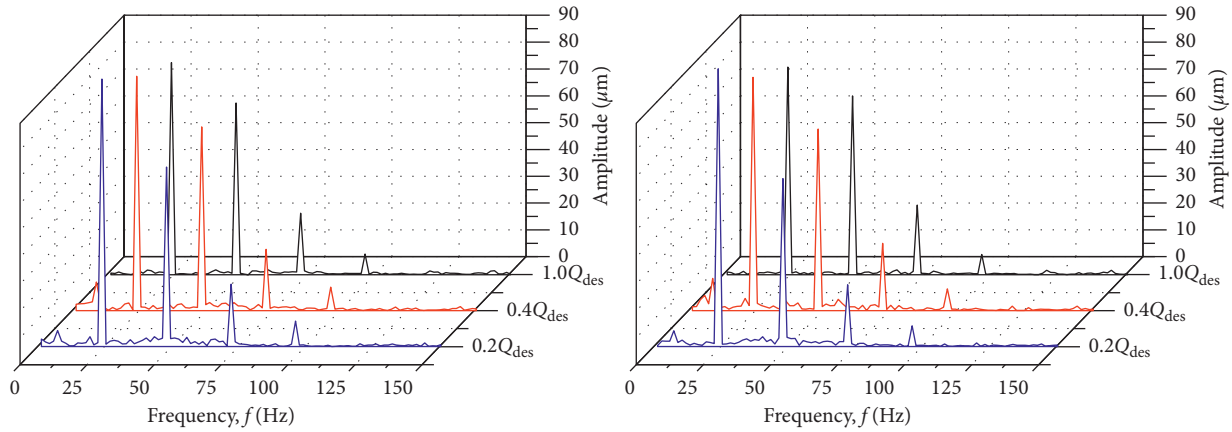

Figure 11: Frequency spectrogram of X and Y direction: (a) X direction. (b) Y direction.

partial load condition is the main reason for the deterioration of shaft system vibration, and the 2X frequency also affects the axis orbit in a low level, while other frequencies have less influence on the shaft vibration. The contribution of imbalance and misalignment to shaft vibration is significant under low flow rate condition.

5. Conclusions

In order to get hold of the relationship between the rotor-stator interaction and the shaft system vibration, the PIV experiment and axis orbit collection of a mixed-flow pump model were carried out under the design flow rate condition and the partial load conditions. The flow fields in the impeller interaction zones were developed based on the PIV technology, and the shaft vibration was measured using the Bentley 408 data acquisition system. In addition, the shaft movements induced by the unsteady rotor-stator interaction flow fields are related to the axis orbit of mixed-flow pump leading to the following conclusions:

Under the partial load conditions, the secondary flow such as the backflow, flow separation, and the unsteady flow of vortexes at various scales appear in the rotor-stator interaction flow field of the mixed-flow pump. Thus, the medium-frequency exciting force and high-frequency exciting force induced by these unstable flows resulting from the rotor-stator interaction are the main factors to worsen the shaft vibration at the power frequency, which causes the imbalance of the shaft system increasing and the rise on the level of the shaft vibration. In order to improve the reliability of the shaft system and life expectancy, the mixed-flow pump should be avoided to operate under the partial load conditions.

The axis orbit frequency domain shows that the radial offset and misalignment of the shaft system increase under the partial load conditions, which means the vibration of the shaft system increases seriously. In addition, the rotor-stator interaction under partial load condition is the main reason for the deterioration of shaft system vibration. Even though the 2X frequency also affects the axis orbit, its strength is in a low level and other frequencies have less influence on the shaft vibration.

Data Availability

All the data used in this paper come from experiment, so the data can be extracted from this paper. Also, everyone could use and access the data and there are no restrictions of these data.

Conflicts of Interest

The authors declare that there are no conflicts of interest regarding the publication of this paper.

Acknowledgments

This work was sponsored by the National Natural Science Foundation of China (nos. 51679111, 51579118, and 51409127), National Key R&D Program Project (no. 2017YFC0403703), PAPD, Six Talents Peak Project of Jiangsu Province (no. HYZB-002), Key R&D Program Project in Jiangsu Province (nos. BE2015119, BE2015001-4, BE2016319, and BE2017126), Natural Science Foundation of Jiangsu Province (nos. BK20161472 and BK20160521), Science and Technology Support Program of Changzhou (no. CE20162004), Key R&D Program Project of Zhenjiang (no. SH2017049), and Scientific Research Start Foundation Project of Jiangsu University (no. 13JDG105).

References

[1] K. Majidi, "Numerical study of unsteady flow in a centrifugal pump," *Journal of Turbomachinery*, vol. 127, no. 4, pp. 363–371, 2005.

[2] F. Meng, J. Pei, and J. Chen, "Effect of two diffuser types of volute on pressure fluctuation in centrifugal pump under part-load condition," in *Proceedings of International Conference on Electrical Engineering and Automation (EEA2016)*, pp. 1–6, Hong Kong, China, June 2017.

[3] W. Li, L. Zhou, W.-D. Shi, L. Ji, Y. Yang, and X. Zhao, "PIV experiment of the unsteady flow field in mixed-flow pump under part loading condition," *Experimental Thermal and Fluid Science*, vol. 83, pp. 191–199, 2017.

[4] S. Christopher and S. Kumaraswamy, "Study of noise and vibration signal for a radial flow pump during performance

test," *Fluid Mechanics and Fluid Power–Contemporary Research*, vol. 12, pp. 853–861, 2017.

[5] T. Kreuz-Ihli, D. Filsinger, A. Schulz et al., "Numerical and experimental study of unsteady flow field and vibration in radial inflow turbines," *Journal of Turbomachinery*, vol. 122, no. 2, pp. 247–254, 1999.

[6] H. Ohashi, H. Imai, and T. Tsuchihashi, "Fluid force and moment on centrifugal impellers in precessing motion," *ASME Fluid Machinery Forum*, vol. 119, pp. 57–60, 1991.

[7] M. Schleer and R. S. Abhari, "Clearance effects on the evolution of the flow in the vaneless diffuser of a centrifugal compressor at part load condition," *Journal of Turbomachinery*, vol. 130, no. 3, pp. 981–991, 2008.

[8] L. Dobšáková, N. Nováková, V. Habán, M. Hudec, and P. Jandourek, "Vibrations of hydraulic pump and their solution," *EPJ Web of Conferences*, vol. 143, article 02017, 2017.

[9] L. Wei, J. Leilei, S. Weidong et al., "Influence of different flow conditions on rotor axis locus of mixed-flow pump," *Transactions of the Chinese Society of Agricultural Engineering*, vol. 32, no. 4, pp. 91–97, 2016.

[10] L. Wei, J. Leilei, S. Weidong et al., "Experimental study on orbit of shaft centerline of mixed-flow pump during starting period," *Journal of Mechanical Engineering*, vol. 52, no. 22, pp. 168–177, 2016.

[11] K. Wang, H. Liu, X. Zhou et al., "Experimental research on pressure fluctuation and vibration in a mixed flow pump," *Journal of Mechanical Science and Technology*, vol. 30, no. 1, pp. 179–184, 2016.

[12] C. Li and B. P. M. van Esch, "Blade interaction forces in a mixed-flow pump with vaned diffuser," in *Proceedings of ASME 2009 Fluids Engineering Division Summer Meeting*, vol. 1, pp. 165–173, Vail, CO, USA, August 2009.

[13] B. P. M. van Esch and L. Cheng, "Unstable operation of a mixed-flow pump and the influence of tip clearance," in *Proceedings of ASME-JSME-KSME Joint Fluids Engineering Conference*, vol. 1, pp. 79–87, Hamamatsu, Japan, July 2011.

[14] B. P. M. van Esch, "Performance and radial loading of a mixed-flow pump under non-uniform suction flow," *Journal of Fluids Engineering*, vol. 131, no. 5, pp. 051101–051107, 2009.

[15] L. Gros, A. Couzinet, and D. Pierrat, "Part load flow and hydrodynamic instabilities of a centrifugal pump: part 1—experimental investigations," in *Proceedings of ASME-JSME-KSME Joint Fluids Engineering Conference*, vol. 28, no. 3, pp. 278–283, Seoul, Korea, 2015.

[16] A. Couzinet, L. Gros, and D. Pierrat, "Part load flow and hydrodynamic instabilities of a centrifugal pump: part 2—numerical simulations," in *Proceedings of ASME-JSME-KSME Joint Fluids Engineering Conference*, vol. 28, no. 3, pp. 278–283, Seoul, Korea, 2015.

[17] H. Ding, F. C. Visser, Y. Jiang, and M. Furmanczyk, "Demonstration and validation of a 3D CFD simulation tool predicting pump performance and cavitation for industrial applications," *Journal of Fluids Engineering*, vol. 133, no. 1, pp. 011101–011114, 2011.

[18] L. Zhou, W. Shi, W. Cao, and H. Yang, "CFD investigation and PIV validation of flow field in a compact return diffuser under strong part-load conditions," *Science China Technological Sciences*, vol. 58, no. 3, pp. 405–414, 2015.

[19] L. Tan, B. Zhu, Y. Wang, S. Cao, and S. Gui, "Numerical study on characteristics of unsteady flow in a centrifugal pump volute at partial load condition," *Engineering Computations*, vol. 32, no. 6, pp. 1549–1566, 2015.

[20] R. K Byskov, C. B. Jacobsen, and N. Pedersen, "Flow in a centrifugal pump impeller at design and off-design conditions—part II: large eddy simulations," *Journal of Fluids Engineering*, vol. 125, no. 1, pp. 73–83, 2003.

[21] N. Pedersen, P. S. Larsen, and C. B. Jacobsen, "Flow in a centrifugal pump impeller at design and off-design conditions—part I: Particle Image Velocimetry (PIV) and Laser Doppler Velocimetry (LDV) measurements," *Journal of Fluids Engineering*, vol. 125, no. 1, pp. 61–72, 2003.

[22] W. Li, L. Ji, W. Shi, X. Jiang, and Y. Zhang, "Vibration characteristics of the impeller at multi-conditions in mixed-flow pump under the action of fluid-structure interaction," *Journal of Vibroengineering*, vol. 18, no. 5, pp. 3213–3224, 2016.

[23] U. Ješe, R. Fortes-Patella, and M. Dular, "Numerical study of pump-turbine instabilities under pumping mode off-design conditions," in *Proceedings of ASME-JSME-KSME Joint Fluids Engineering Conference*, vol. 1, Seoul, Korea, 2015.

[24] Y. S. Yoon and S. J. Song, "Analysis and measurement of the impact of diffuser width on rotating stall in centrifugal compressors," *Journal of Mechanical Science and Technology*, vol. 28, no. 3, pp. 895–905, 2014.

[25] L. Zhang, R. Wang, and S. Wang, "Simulation of broadband noise sources of an axial fan under rotating stall conditions," *Advances in Mechanical Engineering*, vol. 2014, pp. 1–11, 2014.

[26] C. G. Rodriguez, E. Egusquiza, and I. F. Santos, "Frequencies in the vibration induced by the rotor stator interaction in a centrifugal pump turbine," *Journal of Fluids Engineering*, vol. 129, no. 11, pp. 1428–1435, 2007.

[27] R. P. Dring, H. D. Joslyn, L. W. Hardin, and J. H. Wagner, "Turbine rotor-stator interaction," *Journal of Engineering for Power*, vol. 104, no. 4, pp. 729–742, 1982.

[28] W. Qin and H. Tsukamoto, "Theoretical study of pressure fluctuations downstream of a diffuser pump impeller—part 1: fundamental analysis on rotor-stator interaction," *Journal of Fluids Engineering*, vol. 119, no. 3, pp. 647–652, 1997.

[29] H. Wang and H. Tsukamoto, "Fundamental analysis on rotor-stator interaction in a diffuser pump by vortex method," *Journal of Fluids Engineering*, vol. 123, no. 4, pp. 737–747, 2001.

[30] M. Zhang and H. Tsukamoto, "Unsteady hydrodynamic forces due to rotor-stator interaction on a diffuser pump with identical number of vanes on the impeller and diffuser," *Journal of Fluids Engineering*, vol. 127, no. 4, pp. 743–751, 2005.

[31] X. Zhang, P. Wang, X. Ruan, Z. Xu, and X. Fu, "Analysis of pressure pulsation induced by rotor-stator interaction in nuclear reactor coolant pump," *Shock and Vibration*, vol. 2017, Article ID 7363627, 18 pages, 2017.

[32] J. Keller, E. Blanco, R. Barrio, and J. Parrondo, "PIV measurements of the unsteady flow structures in a volute centrifugal pump at a high flow rate," *Experiments in Fluids*, vol. 55, no. 10, p. 1820, 2014.

[33] Y. Chenhong, *The Methods and Judgment of Fault Diagnosis for Centrifugal Pump*, Daqing Petroleum Institute, Daqing, China, 2006.

[34] N. R. Sakthivel, V. Sugumaran, and S. Babudevasenapati, "Vibration based fault diagnosis of monoblock centrifugal pump using decision tree," *Expert Systems with Applications*, vol. 37, no. 6, pp. 4040–4049, 2010.

[35] F. Yang and C. Liu, "Pressure pulsations of the blade region in S-shaped shaft-extension tubular pumping system," *Mathematical Problems in Engineering*, vol. 2014, Article ID 820135, 10 pages, 2014.

[36] Z. Wen-Bin, Z. Xiao-Jun, S. Lu et al., "Purification of rotor axis's orbit based on morphological wavelet," *Journal of Zhejiang University*, vol. 44, no. 8, pp. 1449–1453, 2010.

[37] Y. Wei, W. B. Xu, H. J. Zeng et al., "Rotor axis orbit monitoring based on virtual instrument," *Advanced Materials Research*, vol. 279, pp. 382–387, 2011.

[38] Y. Lin, X. Zhou, W. Zhang, and X. Yang, "Automatic identification of axis orbit based on normalized pattern spectrum," in *Proceedings of Congress on Image and Signal Processing*, vol. 4, pp. 115–119, Sanya, China, May 2008.

[39] X. Yangang, N. Guangwen, Z. Haiying et al., "Axis orbit automatic identification on time-series similarity mining for hydropower units," *Journal of Drainage and Irrigation Machinery Engin*, vol. 35, no. 12, pp. 1054–1057, 2017.

[40] Y. Y. Chen Jian, C. Shu, G. Chen, Y. Yu, and J. Wang, "Automatic identification of pump unit axis orbit based on invariant moments features and neural networks," *Journal of Drainage and Irrigation Machinery Engin*, vol. 29, no. 1, pp. 67–71, 2011.

[41] M. Akioka, A. Miura, T. Orikasa et al., "Dynamic beam pattern control based on shape of large deployable reflector measured with vision metrology in orbit," in *Proceedings of 34th AIAA International Communications Satellite Systems Conference*, Cleveland, OH, USA, October 2016.

[42] P. Xinyu, Y. Zhaojian, Y. Jianxiang, R. Fang, and L. Juanli, "Recognition of torque load for elastic support rotor system based on axis orbit," in *Proceedings of 13th International Conference on Ubiquitous Robots and Ambient Intelligence (URAI)*, pp. 830–835, Xian, China, August 2016.